Journal of Applied Polymer Science

A Dynamically Distributed Reactor Model for Identifying the Flow Fields in Industrial Loop Propylene Polymerization Reactors

Xiong-Fa Yang,[1] Tao Zheng,[2] Li-Ming Che,[2] Zheng-Hong Luo[2]

[1]Key Laboratory of Organosilicon Chemistry and Material Technology of Ministry of Education, Hangzhou Normal University, Hangzhou 310012, People's Republic of China

[2]Department of Chemical and Biochemical Engineering, College of Chemistry and Chemical Engineering, Xiamen University, Xiamen 361005, China

Correspondence to: Z.-H. Luo (E-mail: luozh@xmu.edu.cn)

ABSTRACT: The use of distributed parameter model is becoming a common approach for simulating liquid–solid flow in loop polymerization reactors. However, there are still several issues with it. One of them is the absence of modeling of distributed pressure, as no thermodynamic state-equation is incorporated into the model. In this work, inner pressure of the reactor was associated with temperature using a thermodynamic state-equation for high-pressure liquid. The thermodynamic state-equation was solved together with a dynamically distributed reactor model based on the mass, energy, and momentum conservation as well as polymerization kinetics to predict the dynamic trajectories of component concentration, temperature, pressure, and bulk mass velocity in the reactor. Industrial steady-state data were used for model validation. The application of the model was demonstrated by simulating the effect of recycle ratio on the above distributed reactor parameters. © 2012 Wiley Periodicals, Inc. J. Appl. Polym. Sci. 128: 4302–4313, 2013

KEYWORDS: kinetics; polyolefins; theory; modeling

Received 16 August 2012; accepted 1 October 2012; published online 22 October 2012
DOI: 10.1002/app.38668

INTRODUCTION

Polypropylene (PP) can be produced in various types of reactors, such as autoclave, continuous stirred tank, fluidized-bed reactor (FBR), and tubular loop reactor. Tubular loop reactor is the most frequently used one at present.[1,2] In the loop reactors, polymerization occurs in a liquid phase under a reactor pressure of 3.5–4.5 MPa and the polymer matrix is produced as a solid suspension in the liquid stream, namely a liquid–solid two-phase polymerization system. Propylene polymerization is a highly exothermic reaction where the pressure is difficult to control.[2–6] The quick rise of reactor temperature and pressure usually results in breakage of the reactor and consequent release of flammable fluids.[7,8] In addition, the reactor pressure influences the polymerization rate, feed rate, and product properties.[9–11] Thus, control of reactor pressure and temperature are necessary.[10–12] On the other hand, to achieve an optimum performance for the complete PP preparation process, the reactor should be comprehensively optimized.[13] Because of the complexity of liquid–solid polymerization system, the development of reactor model, from which product information (such as component concentration and density, etc.) as well as flow-field information (such as reactor pressure and temperature, etc.) can be derived in a quantitative fashion, is of critical importance.[14] Furthermore, the occurrence of physical and chemical phenomena at different scales makes the reactor model possess a dynamically distributed nature.[15–19] Therefore, a dynamically distributed reactor model involving a distributed pressure equation would be necessary in order to describe the reactor behavior accurately.[20,21]

To develop a dynamically distributed model, especially a dynamically distributed pressure model, the kinetics, mass, energy, and momentum conservation equations must be solved together with the thermodynamics state-equation for the high-pressure liquid in loop reactors.[21–23]

Most of the papers published on olefin polymerization concerned the heat and mass transfer inside the polymer particles and the reaction mechanism/kinetics.[1–6,21–26] The overall polymerization process combined with the dynamically distributed pressure in the reactors was normally neglected. The first mathematical model developed for the polymerization of propylene in loop reactors appeared in the 1970s[27,28] and used continuous stirred tank reactors (CSTRs) to describe the mixing patterns in these systems. The approach was also used later by Ferrero and

Additional Supporting Information may be found in the online version of this article.

Chioveta[29] and suffered from the limitation that the system must operate at very high recycle ratios in order to guarantee perfect mixing. The models based on this approach can not predict the main flow-field parameters, such as pressure and mass velocity due to the absence of state-equation and momentum conservation equation.[27–29] Zacca and Ray[30,31] were the first to propose a distributed dynamic model to describe the propylene polymerization in loop reactors. However, validation of the model with industrial data was not presented. In addition, the loop reactor was handled as two tubular rectors interconnected and their model is based on the kinetics, mass, energy, and momentum conservation equations.[30,31] However, no reactor pressure data are reported in Zacca and Ray's works.[30,31] Furthermore, Zacca and Ray[30,31] did not describe the discrete process of the momentum conservation equation and the velocity gradient along the loop length. Reginato, Zacca, and Secchi[32] developed a dynamically concentrated model instead of distributed model for liquid-phase polymerization in loop reactors, which is based on the nonideal CSTR model capable of dealing with multisite copolymerization of olefins. In their work, polymer moment balances were used to compute resin properties, such as average molecular weights, polydispersity, and melt flow index, but no reactor pressure and mass velocity data were reported. Pinto et al.[33] presented a dynamically distributed model with a recycle pump in the loop PP reactors and validated with industrial data for the first time based on their previous works.[34–37] The model was able to predict the dynamic trajectories of production rates, melt flow index, and xylene soluble values during grade transitions within the experimental accuracy.[38] Although their model was a distributed model and could predict some variable distributions in loop reactors, there were still no distributed pressure and mass velocity data due to the absences of state-equation and momentum conservation equation in their works.[33–37] Recently, Touloupides et al.[1] developed a comprehensive dynamical mathematical model to describe the dynamic operation of an industrial slurry-phase ethylene-1-hexene copolymerization loop reactor series based on dynamical macroscopic mass and energy conservations for each loop reactor and validated with industrial data. In their model,[1] each loop reactor consisting of loop reactor and settling legs was modeled as an ideal CSTR in series with a semi-continuous product removal unit. Thus, if the recycle ratio is high enough, the reactor can be deemed as an ideal CSTR reactor. It means that all parameters in any position of the reactor are the same in their work. More recently, based on the mass, energy, thermodynamics and kinetics conservations as well as the pipeline equations of the reactors, Luo et al.[39] developed a dynamic model for the prediction of the reactor variables including the pressure in the loop propylene polymerization reactors. However, Luo et al.'s model is still based on the assumption suggested by Touloupides et al.[1] and is lack of momentum conservation equation.[39] Zheng et al.[40] addressed the issue that whether the velocity gradient can be neglected or not. In their work, two dynamically distributed reactor models, either considering or neglecting axial velocity gradient, were presented to examine its effect in tubular loop polymerization reactors. However, as a note, the reactor model used is simplified and the effect of recycle ratio is neglected.

On the basis of the above discussion, it becomes clear that the early modeling efforts in this field were made to account for the detailed aspect of the polymerization kinetics and to predict the polymer properties in reactors. It is also clear that few open reports were on the dynamically distributed reactor model along with incorporating the momentum conservation equation into the kinetic and thermodynamic models.

In this work, based on the mass, energy, momentum, and kinetics conservations as well as the thermodynamic state-equation for high-pressure liquid, a distributed model is developed for the prediction of reactor variables, especially the distributed pressure in loop propylene polymerization reactors. To the best of our knowledge, the present work is the first one aiming at realizing the combination of distributed pressure model and dynamically distributed reactor model along with incorporating the momentum conservation equation and kinetic equation as well as considering the velocity gradient in loop propylene polymerization reactors. Dynamic data from an industrial plant are used for model validation. Particular attentions are paid to the application of the model to identify the flow fields in loop propylene polymerization reactors by simulating the effect of recycle ratio on the distributed reactor parameters.

LOOP REACTOR DESCRIPTION

The Spheripol technology is one of the most widespread commercial methods to be used to produce PP.[41–45] Generally, its key part constitutes of three loop reactors and a FBR. To illustrate this technology, a typical schematic flowsheet of the continuous tubular loop reactors from a chemical plant in China is shown in Figure 1, where the same flowsheet is reported in our previous works.[2,3,39,41,46,47] In addition, some points are listed as follows: first, the technology includes a prepolymerization reactor (R200) and two main polymerization reactors in same volume (R201 and R202), which are sequentially linked together. Second, both R201 and R202 consist of two continuous tubular reactors connected in sequence with each other, namely, they are both closed tubes as a whole, wherein the reacting slurry driven by recycling pumps circulate at high-recycle rates.[2,3,39,41,46,47] In this work, in order to develop a dynamically distributed reactor model, R201 is selected as our studied object.

On the other hand, there are many published papers relating to the loop polymerization reactor (R200, R201 or R202).[2,3,30–33,39,41,46,47] As reported in previous works,[30–32] the loop reactor consists essentially of a main tubular system closed in a loop (see Figure 1). The reaction slurry flows through the pipe impelled by an axial pump. Its cross-sectional area is usually uniform and the reactor must operate free of any obstruction that could interfere with the circulation of the reaction contents. In addition, the basic set-up configuration analyzed here has been presented by Zacca and Ray.[30,31] In short, the loop reactor (R201) is formed by two tubular reactors interconnected. Figure 2 shows a schematic flowsheet representation of the loop reactor model, namely, the physical model of R201. The convention adopted is that the axial coordinate z has its origin at the inlet zone and increases in the same direction of the fluid flow. In addition, from Figure 2, R201 composes of two tubular sections where

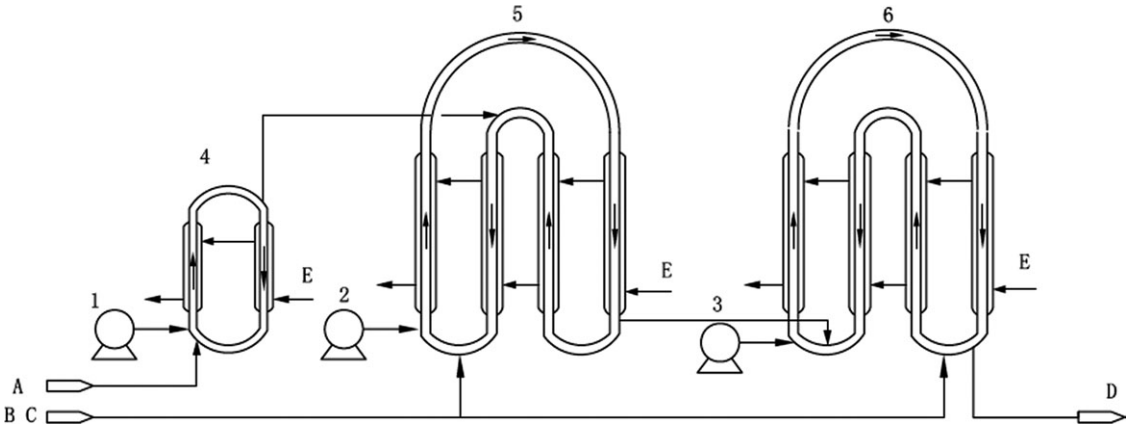

Figure 1. Basell Spheripol-II loop process (China Lanzhou Petrochemical Company of China National Petroleum Corporation). (A—Catalyst; B—Propylene; C—Hydrogen; D—Product; E—Coolant; 1—P200; Pump; 2—P201, Pump; 3—P202, Pump; 4—R200, Pre-polymerization reactor; 5—R201, Main polymerization reactor; 6—R202, Main polymerization reactor).

the cooling water flows into the jacket to remove the reaction heat. Section 1 represents the tubular section that starts at the inlet zone and ends at the outlet zone by following the fluid flow direction, whereas Section 2 represents the recycle portion of the reactor.[30,31] Monomer, fresh catalyst, and hydrogen are introduced into the reactor from the reactor inlet, and polymer slurry in the reactor leaves from the reactor outlet, and the distance between the inlet and outlet is 113 m. The two small tank reactors shown in Figure 2 are not real. However, they can be used to explain material and energy mixture. The two reactors are small enough to neglect component residence time. In practice, they connect the four boundaries (0^+, 0^-, L^+, L^-) of two sections. Accordingly, the following mathematical model is based on this physical model shown in Figure 2.

DYNAMICALLY DISTRIBUTED MODEL

As described above, a dynamically distributed model based on the mass, energy, momentum and kinetics conservations as well as the thermodynamic state-equation was used to describe the flow fields in loop reactors for catalytic propylene polymerization. The velocity gradient was considered via the momentum conservation equation, and the pressure gradient was considered via the thermodynamic state-equation. Furthermore, all the above equations were solved together to comprehensively describe the distributed flow-field parameters in the loop reactors. In what follows, propylene polymerization mechanism and kinetics are first presented. Next, the general model of R201 (Figure 2), the thermodynamic state-equation and the initial and boundary conditions are described, respectively.

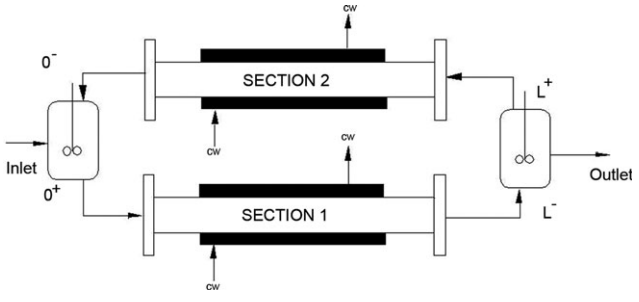

Figure 2. Physical model of R201.

Polymerization Kinetics

Since a concentrated model was developed to simulate the loop polymerization reactors in our previous work,[39] the propylene polymerization mechanism and kinetics were also suggested and validated. Herein, the same propylene polymerization mechanism and kinetics were applied. The main mechanism and kinetic equations are listed in Table I and eqs. (1)–(4).

$$\text{Propagation rate}: \ r_P = k_P[M][C^*], \tag{1}$$

$$\text{transfer rate}: \ r_{tr} = k_{tr}[H_2]^{0.5}[C^*], \tag{2}$$

$$\text{catalyst deactivation rate}: \ r_d = k_d[C^*], \tag{3}$$

$$\text{Arrhenius equation}: \ k = k_0 e^{-E/RT}. \tag{4}$$

In addition, some points must be emphasized: (1) the value of the rate constant for each step is independent on the chain length; (2) the value of the chain initiation rate constant is equal to that of the chain propagation rate constant; (3) the

Table I. Kinetic Mechanism[1–6,15,16,31–41]

Initiation	$C^* + M \xrightarrow{k_{iM}} PP_1^*$
Propagation	$PP_1^* + M \xrightarrow{k_P} PP_2^*$
	.....
	$PP_i^* + M \xrightarrow{k_P} PP_{i+1}^*$
Transfer reaction	
Transfer to hydrogen	$PP_i^* + H_2 \xrightarrow{k_{tr}} PP_i + C^*$
Deactivation reactions	
Spontaneous deactivation	$PP_i^* \xrightarrow{k_d} PP_i + C_d$

chain transfer reaction is assumed to occur spontaneously or through the reaction of active chain with hydrogen; (4) the polymerization rate is also given by eq. (1) considering the propagation reaction as the main consumption of propylene.

Dynamically Distributed Reactor Model

As depicted in Figure 2, the loop reactor here is composed of two tubular reactors interconnected and the tubular reactors were then described according to the axial dispersion model. The recycling pump is much smaller in volume than the loop and it is used to provide recycling-flow momentum of slurry in the loop reactor. Thus, it is ignored according to its volume and can not be ignored from the momentum source of loop as described in the next boundary conditions yet.

According to the above discussion, the most similar study presented in the literature on the mathematical modeling of loop polymerization reactors is that of Zacca and Ray.[30,31] However, the dynamically distributed model proposed in this work is based on the physical model shown in Figure 2 with several modifications. The modifications are discussed by considering the velocity and pressure gradients in the loop reactors here, which are ignored by Zacca and Ray.[30,31] Other assumptions for this model can be found in Refs. 30 and 31. Therefore, the following model equations are made based on the above descriptions and the mass, energy, momentum, and kinetics conservations as well as the thermodynamic state-equation.

Component Material Conservation

According to the axial dispersion model, a molar conservation for a given species in a tubular section of the loop reactor results in:

$$\frac{\partial C_j}{\partial t}+\frac{\partial}{\partial z}(C_j v_z)-D^{(t)}\frac{\partial^2 C_j}{\partial z^2}=R_{C_j}, \tag{5}$$

where, C_j is the molar concentration of species j (monomer, catalyst, hydrogen, and moments of the polymer molar mass distribution) in any tubular section of the loop reactor. In addition, since the catalyst activity decreases as a result of catalyst deactivation, the catalyst concentration herein is the active catalyst concentration. Accordingly, in this work, the catalyst concentration is the active catalyst concentration.

Energy Conservation

The energy conservation is obtained by neglecting energy changes due to expansion work, viscous flow, external fields, radiation, and heat of mixing, which is applied in previous works.[30,31,33–37,48] The differential equation of energy in one spatial dimension can be written as:

$$\left(\frac{\partial T}{\partial t}+\frac{\partial (v_z T)}{\partial z}\right)-\alpha^{(t)}\frac{\partial^2}{\partial z^2}T=\frac{1}{\rho C_P}\left\{\sum_{r=1}^{NR}(-\Delta H)_r R_r+\frac{4K}{D}(T_{\text{cold}}-T)\right\}. \tag{6}$$

Momentum Conservation

In this case, the momentum conservation equation is used to calculate the bulk mass velocity gradient and is reduced to the axial component of the equation of motion in cylindrical coordinates. The application of Zacca and Ray's model results in the following equation:[30,31]

$$\frac{\partial P}{\partial z}=-\rho\left[\frac{\partial v_z}{\partial t}+v_z\frac{\partial v_z}{\partial z}+\frac{v_z^2 f_{\text{fric}}}{R_r}\right]+\frac{4}{3}\mu^{(t)}\frac{\partial^2 v_z}{\partial z^2}. \tag{7}$$

The above momentum conservation equation is included in Zacca and Ray's model, however, no axial velocity gradient was considered in their works.[30,31]

Thermodynamic State-Equation for High Pressure Liquid

As described above, the pressure gradient and corresponding thermodynamic state-equation for high pressure liquid are considered in this work, which is one of the differences from previous distributed reactor models.[30,31,33–37] In addition, in our previous work,[39] we have demonstrated that the increase of propylene density is the essential reason of the pressure rise in loop reactors and the reactor pressure can then be described via the pressure of the liquid propylene. Furthermore, we incorporated one of the most excellent state-equations for high pressure liquid, i.e., the Tait equation of state (EOS), into a concentrated reactor model to describe the reactor pressure. Since the Tait EOS is universal and can be applied in a loop reactor,[49–52] it can be incorporated into the distributed reactor model. The governing equations involved in the EOS are listed in eqs. (8) and (9). The detailed information relating eq. (9) is listed in Supporting Information. For more information regarding the EOS, readers are encouraged to refer to Ref. 39.

$$\frac{1}{\rho}=\sum_{j=1}^{NC}\frac{w_j}{\rho_j}+\frac{w_p}{\rho_P}, \tag{8}$$

$$\phi(P,T,\rho_P)=0, \tag{9}$$

where eq. (8) is obtained directly via the definition of density. According to eq. (9), the slurry density is influenced not only by slurry temperature but also by slurry pressure. However, in Zacca and Ray's works,[30,31] the slurry density is only the function of temperature and the influence of pressure on it is ignored.

Initial and Boundary Conditions

Equations (1)–(9) consist of a closed model, namely, the dynamically distributed reactor model. In addition, the model can be used to predict the component concentration, slurry velocity, temperature, and pressure (slurry density can be described via component concentration or slurry temperature and pressure). However, in order to solve the model, some initial and boundary conditions must be needed.

In this work, the input conditions under certain steady-state operation are considered as the initial conditions (these data are directly presented from control-compute at plant site) and the corresponding initial conditions are listed in eqs. (10)–(15).

$$C_M|_{t=0}=7272.4, \tag{10}$$

$$C_H|_{t=0}=16.48, \tag{11}$$

$$C_C|_{t=0}=0.04905, \tag{12}$$

$$C_{PP}|_{t=0}=6101.34, \tag{13}$$

$$T|_{t=0}=343.54, \tag{14}$$

$$v_z|_{t=0} = 7.65. \quad (15)$$

From Figure 2, the axial dispersion model requires the establishment of two boundary conditions per tubular section since the partial differential equations above are of second order. In this work a closed-closed set of boundary conditions for both tubular sections is similar to that reported by Zacca and Ray with a few modifications.[30,31] The description regarding the selected boundary conditions are listed as follows:

First, four points (Figure 2) are selected to denote four different positions of the two sections, respectively. Namely, 0^+ denotes the boundary after the inlet zone, following the direction of the fluid motion; 0^- denotes the boundary before the inlet zone, following the direction of the fluid motion; L^+ denotes the boundary after the outlet zone, following the direction of the fluid motion; and L^- denotes the boundary before the outlet zone, following the direction of the fluid motion. Correspondingly, the selected boundary conditions are listed as follows.

On the basis of the component material, the energy and the momentum conservation in the inlet stirred-tank reactor, the boundary conditions at L^+ are described via eqs. (16)–(18):

$$\left.\frac{\partial C_j}{\partial t}\right|_{z=0^+} = \frac{(q_{j,F} + (v_z A_x C_j)|_{z=0^-} - (v_z A_x C_j)|_{z=0^+})/(A_x v_z)|_{z=0^+}}{V_{\text{in}}} + R_{C_j}, \quad (16)$$

$$\rho C_P \left.\frac{\partial T}{\partial t}\right|_{z=0^+} = \sum_{r=1}^{NR} (-\Delta H)_r R_r + \frac{UA_x(T_{\text{cold}} - T^{0^+})}{V_{\text{in}}} - \frac{1}{V_{\text{in}}}[q_F \int_{T_F}^{T^{0^+}} C_P dT + \rho^{0^-} v_z^{0^-} A_x \int_{T^{0^-}}^{T(0)} C_P dT], \quad (17)$$

$$v_z|_{z=0^+} = \frac{(v_z A_x)|_{z=0^-} + Q_F}{A_x}. \quad (18)$$

On the other hand, for Section 2 shown in Figure 2, based on the mass conservation equation, the following equation can be obtained:

$$Q_0 = Q_{L^-} - Q_{\text{Rec}}. \quad (19)$$

If Q_o is constant, the recycle ratio is determined by the outlet velocity of Section 1. In practice, the recycle ratio is set around 200, it means that most of the materials flow back into the loop reactor. Accordingly, in Zacca and Ray's works,[30,31] the assumption of $Q_{L^-} = Q_{\text{Rec}}$ was adopted. Furthermore, the velocities in Sections 1 and 2 are the same if their diameters are the same. Therefore, if $Q_{L^-} = Q_{\text{Rec}}$, it means that $Q_o = 0$ and no any materials flow out from the reactor. Obviously, it is unpractical. In this study, eq. (19) is adopted instead of $Q_{L^-} = Q_{\text{Rec}}$ and the recycle ratio (R_{ec}) is defined as eq. (20):

$$\text{R}_{\text{ec}} = Q_{\text{Rec}}/Q_o. \quad (20)$$

Accordingly, the component material concentration and velocity ratio after and before the outlet of Section 1 can be written as:

$$R_{21} = R_{\text{ec}}/(1 + R_{\text{ec}}) \quad (21)$$

The boundary conditions at L^+ can be described via eqs. (22)–(24):

$$C_j|_{z=L^+} = R_{21} C_j|_{z=L^-}, \quad (22)$$

$$T|_{z=L^+} = T|_{z=L^-}(\rho C_P)|_{z=L^-}/(\rho C_P)|_{z=L^+}, \quad (23)$$

$$v_z|_{z=L^+} = \sqrt{2gH_e} R_{21} v_z|_{z=L^-}. \quad (24)$$

Here, we must emphasize that the axial pump can not be ignored in this model although it is not described in Figure 2. In practice, in this model, the pump is considered as the production of momentum via eq. (24), which shows that the component materials are recycled from the outlet and accelerated by the axial pump.

On the other hand, for a closed outlet boundary, the mass, energy and momentum fluxes must be zero at the outlet.[30,31] Accordingly, the boundary conditions at 0^- and L^- are described via eqs. (25) and (26), respectively.

$$\frac{\partial AA}{\partial z}|_{z=0^-} = 0, \quad (25)$$

$$\frac{\partial AA}{\partial z}|_{z=L^-} = 0, \quad (26)$$

where, AA is distribution parameter ($AA = C_j$, T, and v_z).

MODEL IMPLEMENTATON AND PARAMETER ESTIMATION

Equations (1)–(30) include a set of coupled, nonlinear partial differential and algebraic equations. The above partial differential equations were first discretized to algebra equations by the Crank-Nicholson method. The algebra equations obtained were then solved as an FSOLVE-function provided in Matlab 6.5 software. To solve the model, the kinetic constants of the model must be estimated. The kinetic constants were estimated from the plant data. Our former models had already been thoroughly validated against data.[39,41] The estimation method of the kinetic constants was also made in our previous works.[39,41] In addition, as described below, the catalyst used in this work is the same as that reported in our previous work. Here, the same estimation method and similar values for the kinetic constants are applied. In addition, some thermodynamic property parameters and plant data related to the model must also be obtained in advance. The estimation of main thermodynamic property parameters (including viscosity and axial dispersion coefficient) was also done in our previous work[39] and the same estimation method was used in this work. The finally adopted kinetic constants are listed in Table II, and the plant data are shown in Table III. In addition, the solution procedure of the model is illustrated in Figure 3. We still point out that the obtained plant data is at the outlet and inlet positions described in Figure 2.

The plant process of the propylene polymerization is a classical slurry polymerization process in the presence of the fourth generation Ziegler-Natta catalyst.

RESULTS AND DISCUSSION

Comparison Between Industrial Data and Simulated Data

By substituting the thermodynamic properties (refer to Ref. 42) and the kinetic constants (Table II) for related terms in eqs. (1)–(30) respectively, the simulated results are obtained. In this work, at the initial state of R201, the loop works under conditions listed in eqs. (10)–(15), which are derived from a real

Table II. Kinetic Constants[39,41]

Kinetic constants	Computational equation, $k = k_0\exp(-E/RT)$
k_{iM}	$k_{iM} = 4.97 \times 10^7 \exp(-51900/RT)$
k_p	$k_p = 4.97 \times 10^7 \exp(-51900/RT)$
k_{tr}	$k_{tr} = 4.4 \times 10^3 \exp(-51900/RT)$
k_d	$k_d = 7.92 \times 10^3 \exp(-51900/RT)$

industrial data. Therefore, these conditions [eqs. (10)–(15)] can be used as the initial values for the current model to calculate parameter distributions.

Figures 4 and 5 illustrate the predicted reactor parameter distributions along the axes in R201. In addition, in order to describe these parameter gradients clearly, the simulated profiles at certain time (i.e., the constant reactor parameters can be obtained since the time and $t = 50{,}000$ s in this study) are also obtained and are illustrated Figure 6 (main reactor parameters not all at the time are listed here). The maximum and minimum values for these reactor parameters shown in Figure 6 are specially listed in Table IV. Meanwhile, the above reactor parameters under steady-state operation conditions (the conditions are the same as the above simulation conditions) were also collected from the industrial R201 selected in this work (see also Table IV, in addition, Figures 4–6 will be discussed in the next section).

Table IV illustrates the comparisons between the industrial and simulated data under certain operation conditions in R201. As described in Table IV, the industrial reactor parameter data, such as the bulk mass velocity, the pressure, the monomer concentration and the solid mass fraction, are in the range of the simulation parameter data. In addition, all these ranges are small. It means that a good agreement between the industrial data and the simulated results is obtained. Furthermore, the above also shows that the main reactor parameter gradients are small at $R_{ec} = 170$, which will be described and discussed later.

The Effect of Recycle Ratio on the Flow Field and Its Identification

As shown in Figures 4 and 5, these dynamically distributed parameters (i.e., component concentrations, temperature, pressure and bulk mass velocity) in R201 are expressed via three-dimensional drawings at $R_{ec} = 170$. Furthermore, Figures 4 and 5 are used to demonstrate the dynamically distributed nature of the flow field in R201.

Table III. Input Parameters from Plant[39]

Parameters	Values
V_{201}/m^3	66
Jacket water temperature (T_{cold})/°C	62.85
G_H /(kg/h)	0.51
G_M/(kg/h)	2.418×10^4
T_{in}/°C	29.5
P_{in}/MPa	5.358
$Q_o/(m^3/s)$	0.0129512
Heat transfer coefficient (K)/(W/(m^2·K))	1600

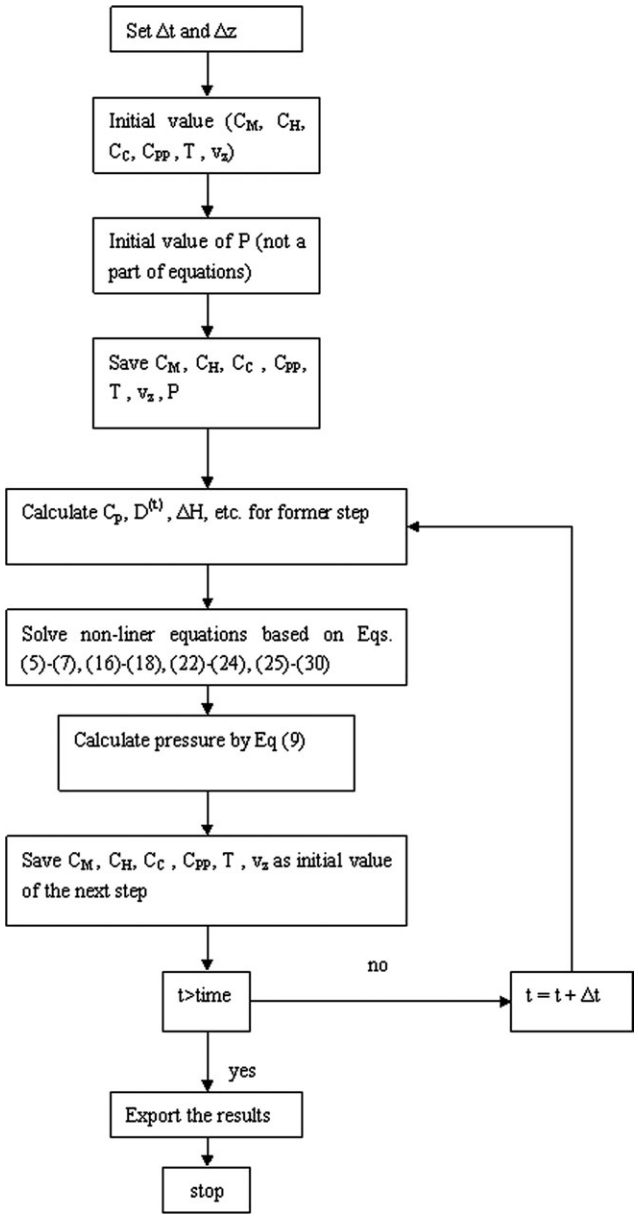

Figure 3. Flowsheet of dynamical distributed model in this study.

From Figures 4 and 5, all of the parameter values at each axial position of R201 change from one steady state to another steady state with the polymerization proceeding, which means that the polymerization is dynamical during the two steady states. The interval between the two steady states is about 30,000 s as described in Figures 4 and 5. Therefore, in the next study, the simulation data at $t = 50{,}000$ s (after 30,000 s) are selected to evaluate the effect of R_{ec} on the flow field in R201. Furthermore, according to Figures 4 and 5, one can also find that these changes are different with each other for different parameters. With the polymerization proceeding during the two steady states, the monomer concentration and the pressure at each

Applied Polymer SCIENCE

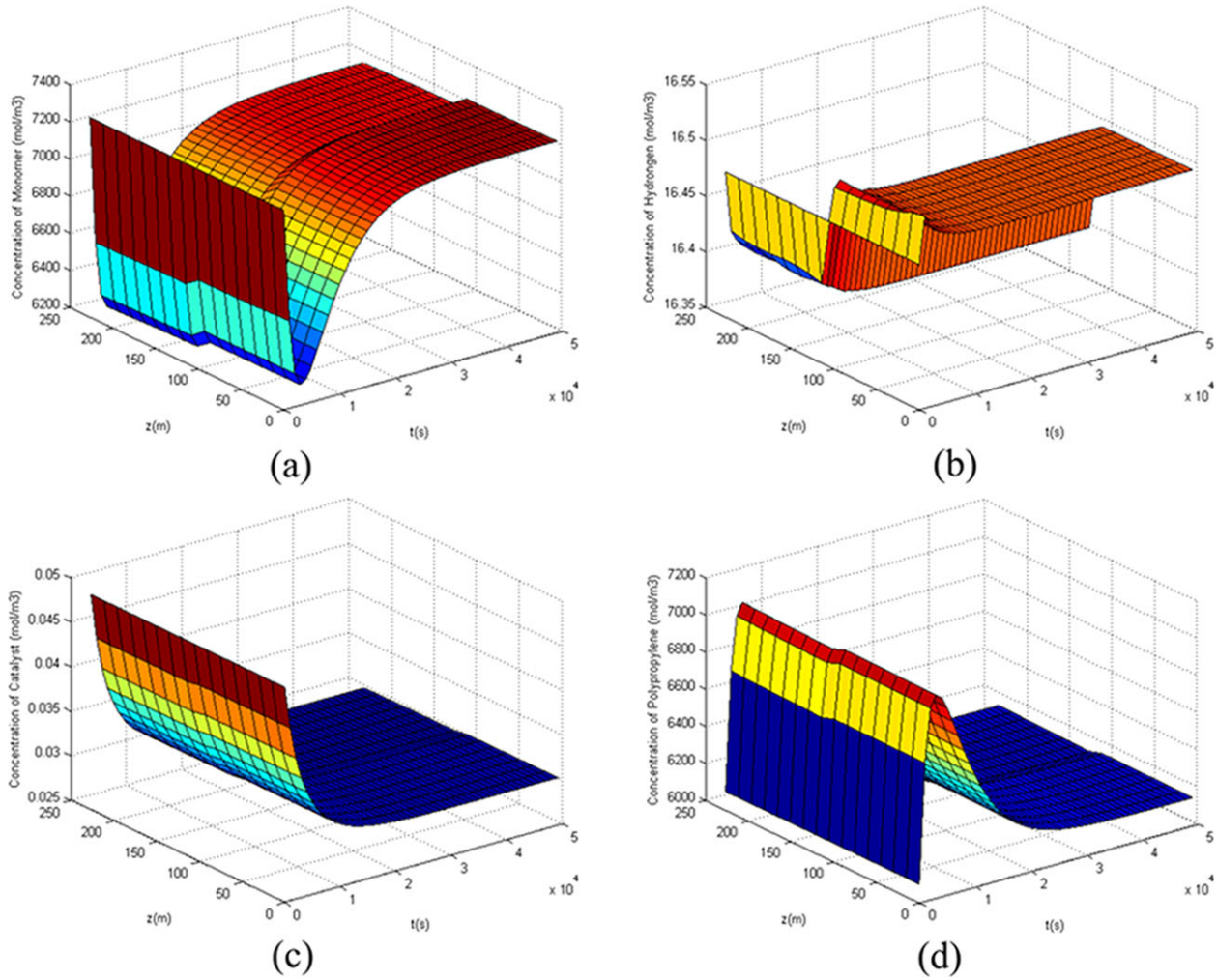

Figure 4. (a) Monomer concentration profile. (b) Hydrogen concentration profile. (c) Catalyst concentration profile. (d) Polypropylene concentration profile. ($T = 69.39°C$, $P = 4.034$ MPa, $v_z = 7.65$ m s^{-1}, Rec = 170, $\rho = 561.7$ kg m^{-3}, $G_H = 0.51$ kg h^{-1}, $G_M = 2.418 \times 104$ kg h^{-1}, $T_{in} = 29.5°C$, $P_{in} = 5.358$ MPa). [Color figure can be viewed in the online issue, which is available at wileyonlinelibrary.com.]

axial position of R201 decrease to minimums quickly and increase to constant values hereafter as described in Figures 4(a) and 5(b). On the contrary, Figures 4(d) and 5(a) show that the PP concentration and the reactor temperature both increase to maximums quickly and decrease to constant values hereafter with the polymerization proceeding during the two steady states. In addition, Figures 4(b,c) demonstrate that both the concentrations of hydrogen and catalyst decrease to constant values with the polymerization proceeding during the two steady states. Figure 4(b) demonstrates that the concentration of hydrogen decreases little with time, as hydrogen is used to regulate average molecule weight of polymers and has weak influence on the polymerization reaction. It means that hydrogen does not influence the generation rate of polypropylene. Compared with that in Figure 4(b,c) illustrates that the concentration of catalyst decreases obviously with the reaction proceeding. In practice, based on eq. (3), one knows that the catalyst activity decreases and the deactivation rate follows a first-class equation. Different from Figures 4 and 5(a)–(c), Figure 5(c) shows that the bulk mass velocity fluctuates slightly during the two steady states. Besides the above results, next, when fixing the polymerization time, namely, at every instant of time, Figures 4 and 5 demonstrate the occurrence of small gradients along the axial direction in R201 as would be expected at $R_{ec} = 170$ (a very high recycle condition). Furthermore, as described in Figures 4 and 5, all these parameter gradients in the middle of the axis are the most notable. In practice, the above results involving the monomer concentration gradient are adjacent to those reported in Zacca and Ray's works.[30,31] However, there are still some different results between in this work and Zacca and Ray's works.[30,31] Zacca and Ray obtained that the loop reactor was fairly uniform presenting almost flat monomer concentration profiles along its axial distance at every instant of time at high R_{ec} ($R_{ec} = 30$). Therefore, they suggested that the loop reactor would behave as a CSTR for R_{ec} above ~ 30.[30,31] In our simulation results, even at $R_{ec} = 170$, although the loop reactor is in total uniform presenting almost flat parameter profiles (including monomer concentration profile) along its axial

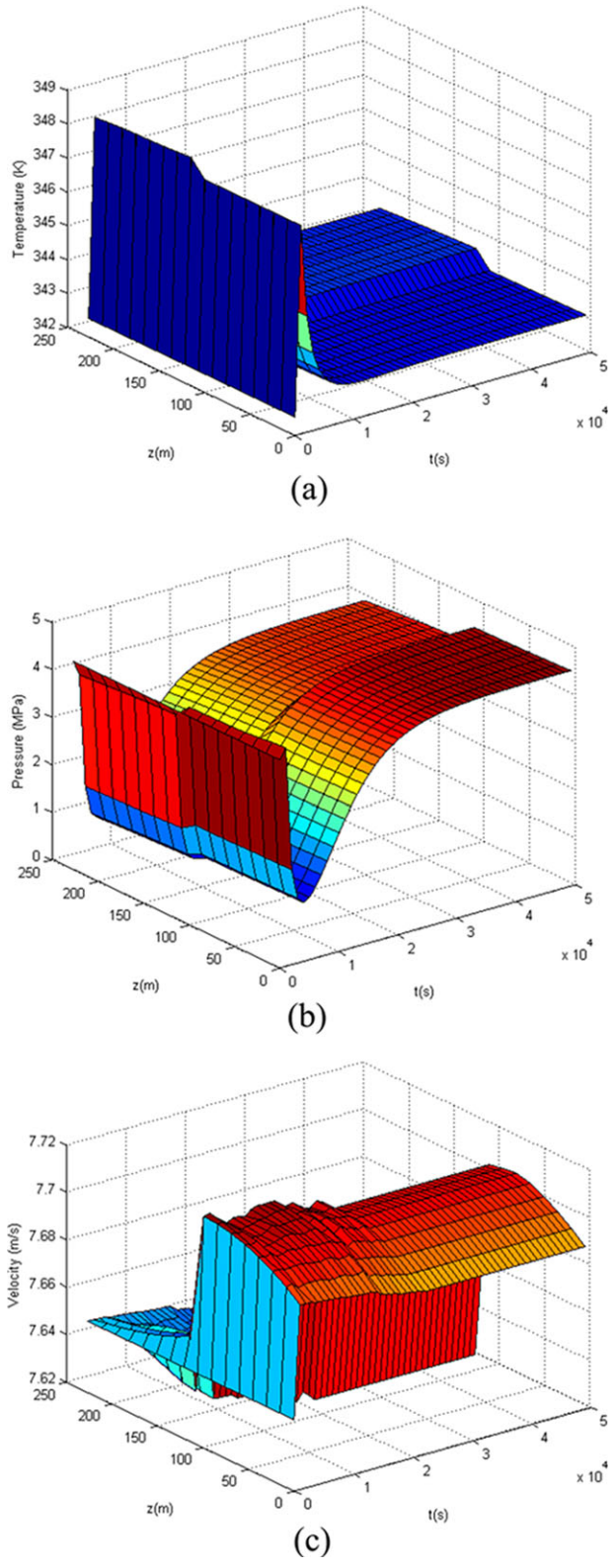

Figure 5. (a) Temperature profile. (b) Pressure profile. (c) Bulk mass velocity profile. ($T = 69.39°C$, $P = 4.034$ MPa, $v_z = 7.65$ m s^{-1}, Rec = 170, $\rho = 561.7$ kg m^{-3}, $G_H = 0.51$ kg h^{-1}, $G_M = 2.418 \times 104$ kg h^{-1}, $T_{in} = 29.5°C$, $P_{in} = 5.358$ MPa). [Color figure can be viewed in the online issue, which is available at wileyonlinelibrary.com.]

distance at every instant of time, the parameter gradients still exist in the middle of the axis.

In order to further demonstrate the above differences, the effects of R_{ec} on the axial flow field in R201 at $t = 50{,}000$ s are simulated via the above model and the main simulation results are shown in Figure 6.

First, Figure 6 prove that the gradients are the most obviously at the outlet of axis in R201 at all selected recycle ratios ($R_{ec} =$ 10, 15, 50, 170, and 500). As mentioned in Figure 2, the two tubes (Section 1 and Section 2) are linked with each other. The inlet of Section 2 is linked to the outlet of Section 1. If no any material/slurry flows out from R201, the above two points, i.e., the inlet position of Section 2 and the outlet of Section 1 will be the same. However, when a small fraction of slurry flows out from R201, they will recycle into Section 2 with the same diameter as that of Section 1. As a result, the monomer concentration in the above joint from the outlet of Section 1 to the inlet of Section 2 decreases, which is exactly the middle of axis in R201. Accordingly, the temperature increases and both the pressure and bulk mass velocity in the joint decrease according to the tait EOS. In addition, since there are the above flowing out from R201 (Section 1) and recycling into R201 (Section 2), the parameters in both Sections 1 and 2 will change. However, the change mechanisms and degrees in this joint and in Sections 1 and 2 are different, As is shown in eqs. (5)–(7), these component concentrations and temperature are influenced by the united-function of reaction and diffusion, the temperature is also influenced by the Jacket water temperature, and the velocity is influenced by the united-function of diffusion and wall-friction. However, these influence factors mentioned above can not cause great parameter gradient along the axis. Due to the direct action as the joint, the change degree in the joint is the most obviously. Next, as described in Figure 6, comparing with the other parameter gradients, the bulk mass velocity gradient along the reactor is the most unconspicuous. Namely, the circumfluence amount has the smallest influence on the velocity since the velocity is directly linked to the momentum equation [eq. (7)], which depends on the axial pump power not its flux. However, the other parameters (component concentrations, temperature, and pressure) are influenced not only by the momentum but also the flux. On the other hand, as described in Figure 6, it is easy to find that all parameters along the axes change toward flat with the increase of R_{ec}. However, it is difficult to determine the critical value corresponding to the case that the parameters along the axis are nearly the same and the reactor model can be handled as a CSTR model. In our viewpoint and based on Figure 6, we recommend that 50 as the critical value of R_{ec}. In practice, the parameters along the axis except in the middle of axis in R201 are nearly the same, which validates the conclusion that the loop reactor will behave as a CSTR model for recycle ratios above 30.[30,31] Namely, here, we adopt this dynamical distributed model to distinguish the CSTR model can be adopted in the loop propylene polymerization reactor for recycle ratios above 50. This rationality of the CSTR model is validated not only by the monomer concentration profile but also temperature, pressure and velocity profiles along the axis. Finally, it is obvious that the monomer concentration decreases with the

Applied Polymer SCIENCE

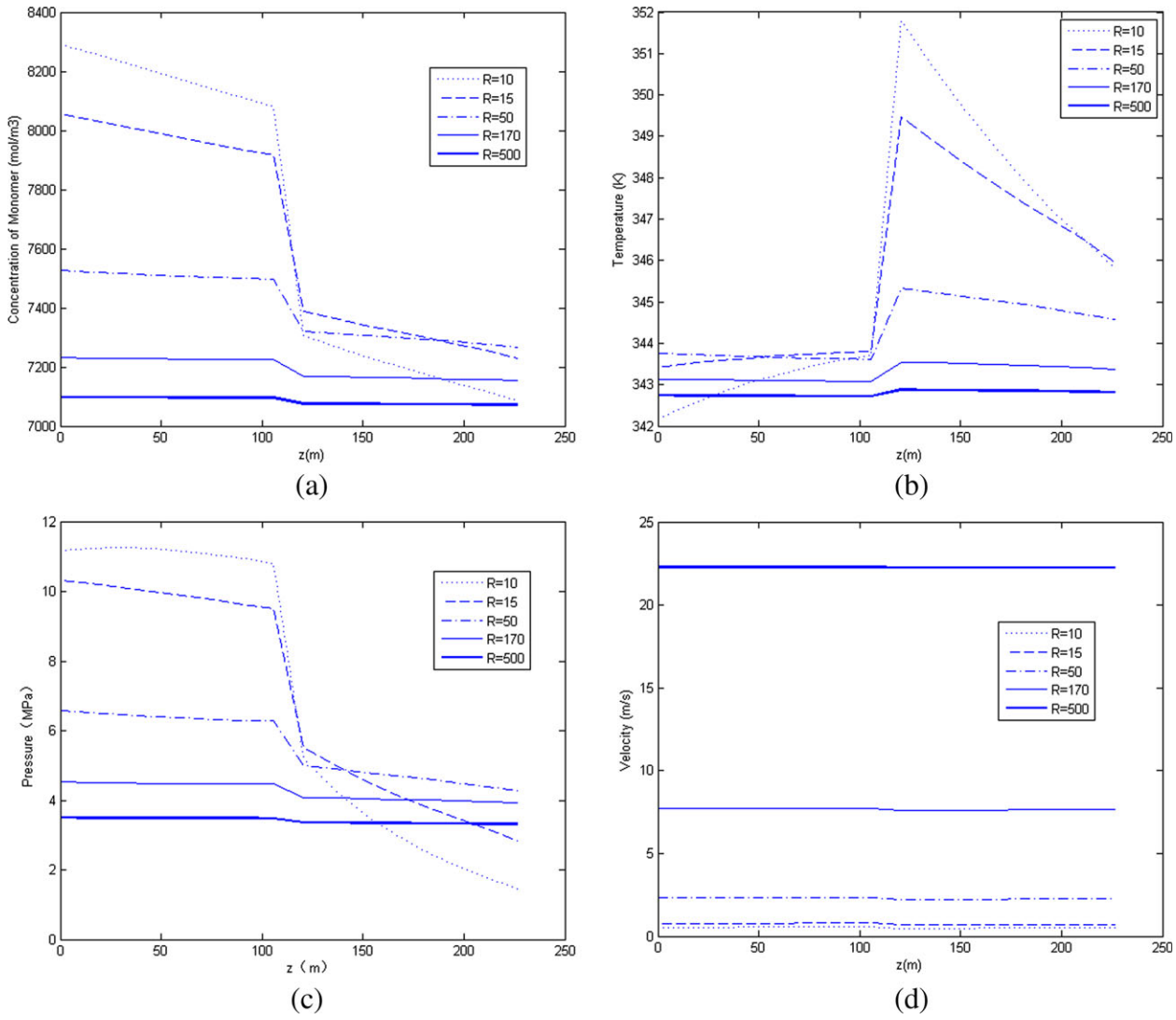

Figure 6. (a) Monomer concentration distributions at different recycle ratios. (b) Temperature distributions at different recycle ratios. (c) Pressure distributions at different recycle ratios. (d) Bulk mass velocity distributions at different recycle ratios. (t = 50,000 s, T = 69.39°C, P = 4.034 MPa, ρ = 561.7 kg m^{-3}, G_H = 0.51 kg h^{-1}, G_M = 2.418 × 104 kg h^{-1}, T_{in} = 29.5°C, P_{in} = 5.358 MPa). [Color figure can be viewed in the online issue, which is available at wileyonlinelibrary.com.]

increase of recycle ratio, which means the monomer conversion increases. Accordingly, a more perfectly mixing and a more effective reaction in R201 generate.

CONCLUSIONS

An improved dynamically distributed model was developed to describe the dynamics of the polymerization of olefins in a loop reactor using Ziegler-Natta catalysts. In this model, the thermodynamic state-equation was solved together with a dynamically distributed reactor model based on the mass, energy, and momentum conservation as well as polymerization kinetics to predict the dynamic trajectories of component concentration, temperature, pressure, and bulk mass velocity in the reactor. Industrial data from certain China plant were used for model validation. The application of the model was demonstrated by

Table IV. Comparison Between the Industrial and Simulation Data

	Velocity (m/s)	Temperature (K)	Pressure (MPa)	Monomer concentration (mol/m^3)	Solid hold-up
Industrial data	7.65	342.54	4.034	7272.4	45.6%
Simulation data	7.62-7.7	343.1-343.55	3.921-4.522	7254-7230	45.9-46.5%

R_{ec} = 170.

simulating the effect of recycle ratio on the above distributed reactor parameters. Following conclusions can be drawn based on the simulation results:

1. At each axial position of the loop reactor, all reactor parameters, including the components, temperature, pressure, and bulk mass velocity, change during two steady states and these changes are different with each other for different parameters. Among them, the bulk mass velocity fluctuates slightly during the two steady states.
2. The simulation results demonstrate the occurrence of small gradients along the axial direction in the loop reactor at $R_{ec} = 170$. The gradients in the middle of the axis are the most.
3. With the increase of recycle ratio, all reactor parameters along the axes change toward flat. However, it is difficult to determine the critical value corresponding to the case that the parameters along the axis are nearly the same and the reactor model can be handled as a CSTR model. The loop reactor works as a CSTR for recycle ratios above ~ 50. The rationality of the CSTR model is validated not only by the monomer concentration profile but also temperature, pressure, and velocity profiles along the axis.

ACKNOWLEDGMENTS

The authors thank the National Natural Science Foundation of China (No. 21076171), the National Ministry of Science and Technology of China (No. 2012CB21500402) and the State-Key Laboratory of Chemical Engineering of Tsinghua University (No. SKL-ChE-10A03) for supporting this work. The authors also thank the anonymous referees for comments on this manuscript.

NOMENCLATURE

General

A_x [m^2]	cross-sectional area square
C_d [−]	deactivation catalyst site
C^* [−]	activated catalyst site
C_j [mol m^{-3}]	component material concentration
C_P [J·(kg K)$^{-1}$]	slurry heat capacity
C_{PM} [J·(kg K)$^{-1}$]	propylene heat capacity
C_{PP} [J·(kg K)$^{-1}$]	polypropylene heat capacity
C_M [mol m^{-3}]	concentration of propylene
C_H [mol m^{-3}]	concentration of hydrogen
C_C [mol m^{-3}]	concentration of catalyst
C_{PP} [mol m^{-3}]	concentration of polypropylene
D [m]	loop reactor diameter
$D^{(t)}$ [m^2 s^{-1}]	axial dispersion coefficient
E [J mol^{-1}]	active energy
f_{fric} [−]	friction factor
g [m^2 s^{-1}]	acceleration of gravity
G_M [kg s^{-1}]	influent mass flow of propylene
G_{H_2} [kg s^{-1}]	influent mass flow of hydrogen
H_e [W]	axial pump power
H_2 [−]	hydrogen
k [−]	reaction rate constants corresponding to eqs. (1)–(3)
K [W m^{-2} K^{-1}]	gross heat-exchange coefficient
k_{iM} [L·(mol·s)$^{-1}$]	monomer-initiation rate
Kd[s^{-1}]	chain termination rate constant
k_p [L·(mol s)$^{-1}$]	chain propagation rate constant
k_{tr} [L·(mol s)$^{-1}$]	rate constant of chain transfer to hydrogen
k_0 [−]	pre-exponential factors corresponding to eqs. (1)–(3)
m [kg]	mass of slurry
M [−]	propylene
NC [−]	number of components
NR [−]	number of reactions
P [MPa]	pressure of propylene
P^0 [Pa]	saturation pressure of propylene
Pr [−]	reduced pressure of propylene
P_r^0 [−]	saturation reduced pressure of propylene
P_c [−]	critical pressure of propylene P_a
PP_i (i = 1, 2, 3, ...) [−]	polymer chain containing i segments
PP_i^* (i = 1, 2, 3, ...) [−]	active polymer chain containing i segments
q_F [kg s^{-1}]	slurry feed flow rate
$q_{j,F}$ [mol s^{-1}]	feed flow rate of component material j
Q [mol s^{-1}]	volumetric flow rate
Q_F [mol s^{-1}]	feed volumetric flow rate
Q_{rec} [mol s^{-1}]	recycle volumetric flow rate
r_p [mol·(L s)$^{-1}$]	polymerization rate
r_{tr} [mol·(L s)$^{-1}$]	chain transfer rate
r_d [mol·(L s)$^{-1}$]	catalyst deactivation rate
R_r [m]	radius of reactor
R [J·(kg mol)$^{-1}$]	gas constant
R_{C_j} [J·(kg mol)$^{-1}$]	producing rate of component j
R_{21} [−]	slurry concentration ratio between inlet of Section 2 and outlet of Section 1
R_{ec} [−]	recycle ratio
t [s]	time
T [K]	temperature of propylene
T_b [K]	boiling point of propylene
T_{br} [−]	reduced temperature factor of propylene (T_b/T_c)
T_c [K]	critical temperature of propylene
T_{cold} [K]	cooling water temperature
T_F [K]	feed temperature
T_r [K]	reduced temperature of propylene
V [m^3]	reactor volume
V_{in} [m^3]	inlet volume
w_j [−]	mass fraction of component j
w_P [−]	mass fraction of polypropylene
v_z [m s^{-1}]	bulk mass velocity
z [m]	axial distance from the inlet

Greek letters

ρ_M [kg m^{-3}]	propylene density
ρ_P [kg m^{-3}]	polypropylene density
ρ [kg m^{-3}]	slurry density

ω_0 [−]	compressibility factor
υ_M [m^3 kg^{-1}]	specific volume of propylene
υ^0 [m^3 mol^{-1}]	saturation specific volume of propylene
$\alpha^{(t)}$ [m^3 kg^{-1}]	thermal dispersion coefficient
ω_P [−]	acentric factor
ζ [−]	configuration factor
$\mu^{(t)}$ [cp]	viscosity of slurry

Superscript

+ [−]	forepart of boundary
− [−]	back end of boundary

Subscript

o [−]	outlet
in [−]	inlet
p [−]	propagation
tr [−]	transfer
d [−]	deactivation
j [−]	reactants ($j = 1-4$ represent monomer, hydrogen, catalyst and polypropylene, respectively)

REFERENCES

1. Touloupides, V.; Kanellopoulos, V.; Pladis, P.; Kiparissides, C.; Mignon, D.; Van-Grambezen, P. *Chem. Eng. Sci.* **2010**, *65*, 3208.
2. Luo, Z. H.; Su, P. L.; You, X. Z.; Shi, D. P.; Wu, J. C. *Chem. Eng. J.* **2009**, *146*, 466.
3. Zacca, J. J.; Debling, J. A.; Ray, W. H. *Chem. Eng. Sci.* **1996**, *51*, 4859.
4. Luo, Z. H.; Wen, S. H.; Zheng, Z. W. *J. Chem. Eng. Jpn.* **2009**, *42*, 576.
5. Hatzantonis, H.; Goulas, A.; Kiparissides, C. *Chem. Eng. Sci.* **1998**, *53*, 3251.
6. Yiannoulakis, H.; Yiagopoulos, A.; Kiparissides, C. *Chem. Eng. Sci.* **2001**, *56*, 917.
7. Luft, G.; Broedermann, J.; Scheele, T. *Chem. Eng. Technol.* **2007**, *30*, 695.
8. Pellegrini, L.; Biardi, G.; Caldi, M. L.; Monteleone, M. R. *Ind. Eng. Chem. Res.* **1997**, *36*, 3075.
9. Heuvelsland, A.; Wichmann, S.; Schellenberg, J. *J. Appl. Polym. Sci.* **2007**, *106*, 354.
10. Mirzaei, A.; Vakili, M.; Tafi, N. *J. Appl. Polym. Sci.* **2007**, *105*, 2703.
11. Ahmed, T. S.; DeSimone, J. M.; Roberts, G. W. *Macromolecules* **2008**, *41*, 3086.
12. Bell, K.; Morris, S. D. *J. Loss Prevent Proc.* **1992**, *5*, 160.
13. Wang, Y. N.; Xu, Y. Y.; Li, Y. W.; Zhao, Y. L.; Zhang, B. *J. Chem. Eng. Sci.* **2003**, *58*, 867.
14. Xie, T. Y.; McAuley, K. B.; Hsu, J. C. C.; Bacon, D. W. *Ind. Eng. Chem. Res.* **1994**, *33*, 449.
15. Dompazis, G.; Kanellopoulos, V.; Toulopides, V.; Kiparissides, C. *Chem. Eng. Sci.* **2008**, *63*, 4735.
16. Chen, Y.; Liu, X. G. *Polymer* **2005**, *46*, 9434.
17. Oliveira, A. G.; Muniz, P. C.; Melo, P. A.; Pinto, J. C. *Polym. React. Eng.* **2003**, *11*, 159.
18. Li, J. B.; Liu, X. G. *J. Appl. Polym. Sci.* **2011**, *119*, 3093.
19. Liu, X. G. *Chinese J. Chem. Eng.* **2007**, *15*, 545.
20. Fisher, H. G.; Melhem, G. A.; Levin, M. E.; Leung, J. C. In: International Symposium on Runaway Reactions, Pressure Relief Design, and Effluent Handling, New Orleans (USA). **1998**, p 39.
21. Fan, R.; Fox, R. O.; Muhle, M. E. In: The 12th International Conference on Fluidization-New Horizons in Fluidization Engineering: Vancouver (Canada), **2007**, p 993.
22. Soares, J. B. P.; Hamielec, A. E. *Polym. React. Eng.* **1996**, *4*, 153.
23. Soares, J. B. P.; Hamielec, A. E. *Polym. React. Eng.* **1995**, *3*, 261.
24. Shamiri, A.; Hussain, M. A.; Mjalli, F. S.; Mostoufi, N. *Chem. Eng. J.* **2010**, *16*, 240.
25. Shamiri, A.; Hussain, M. A.; Mjalli, F. S.; Mostoufi, N.; Shafeeyan, M. S. *Chem. Eng. Sci.* **2011**, *66*, 1189.
26. Shamiri, A.; Hussain, M. A.; Mjalli, F. S.; Mostoufi, N. In: The 2th International Conference on Chemical, Biological and Environmental Engineering (ICBEE): Cairo (Egypt). **2010**, p 114.
27. Uvarov, B. A.; Tsevetkova, V. I. *Polim Protsessy Appar.* **1974**, 165.
28. Lepski, D. M.; Inkov, A. M. Mathematical modeling of polymerization of propylene in loop reactors. *Sb. Tr. Vses. Ob'edin. Neftckhlim* **1977**, *13*, 34.
29. Ferrero, M. A.; Chiovetta, G. *Polym. Plast. Technol. Eng.* **1990**, *29*, 263.
30. Zacca, J. J. Distributed parameter modeling of the polymerization of olefins in chemical reactors. Ph. D. Thesis, University of Wisconsin, Madison, Wisconsin, **1995**.
31. Zacca, J. J.; Ray, W. H. *Chem. Eng. Sci.* **1993**, *48*, 3743.
32. Reginato, A. S.; Zacca, J. J.; Secchi, A. R. *AIChE J.* **2003**, *49*, 2642.
33. de Lucca, E. A.; Filho, R. M.; Melo, P. A.; Pinto, J. C. *Macromol. Symp.* **2008**, *271*, 8.
34. Melo, P. A.; Pinto, J. C.; Biscaia, E. C., Jr. *Chem. Eng. Sci.* **2001**, *56*, 2703.
35. Melo, P. A.; Biscaia, E. C., Jr.; Pinto, J. C. *Chem. Eng. Sci.* **2001**, *56*, 6793.
36. Melo, P. A.; Biscaia, E. C., Jr.; Pinto, J. C. *Chem. Eng. Sci.* **2003**, *58*, 2805.
37. Latado, A.; Embirucu, M.; Mattos, Neto. A. G.; Pinto, J. C. *Polym. Test.* **2001**, *20*, 419.
38. Machado, F.; Pinto, J. C. *Macromol. React. Eng.* **2011**, *5*, 129.
39. Luo, Z. H.; Su, P. L.; Wu, W. *Ind. Eng. Chem. Res.* **2010**, *49*, 11232.
40. Zheng, T.; Jian, C. W.; Luo, Z. H. *Asia-Pacific J. Chem. Eng.* **2012**, DOI:10.1002/apj.1673.
41. Luo, Z. H.; Zheng, Y.; Cao, Z. K.; Wen, S. H. *Polym. Eng. Sci.* **2007**, *47*, 1643.

42. Asteasuain, M.; Brandolin, A. *Comput. Chem. Eng.* **2008**, *32*, 396.
43. Zacca, J. J.; Debling, J. A. *Chem. Eng. Sci.* **2001**, *56*, 4029.
44. Choi, K. Y.; Ray, W. H. *J. Macromol. Sci. Part C: Polym. Rev.* **1985**, *25*, 1.
45. Choi, K. Y.; Ray, W. H. *J. Macromol. Sci. Part C: Polym. Rev.* **1985**, *25*, 57.
46. Luo, Z. H.; Wen, S. H.; Shi, D. P.; Zheng, Z. W. *Macromol. React. Eng.* **2010**, *4*, 123.
47. Zheng, Z. W.; Shi, D. P.; Su, P. L.; Luo, Z. H.; Li, X. *J. Ind. Eng. Chem. Res.* **2011**, *50*, 322.
48. Froment, G.; Bischoff, K. B. Chemical Reactor Analysis and Design, 2nd ed.; Wiley: New York, **1990**.
49. Hirschfelder, J. Q.; Curtis, C. F.; Bird, R. B. Molecular of Gases Liquid; Wiley: New York, **1954**.
50. Tong, J. S. Chemical Engineering Thermodynamics. Beijing: Tsinghua University Press Qinghua University Press (Chinese) **1995**.
51. Vargaftik, N. B. Tables on the Thermo Physical Properties of Liquids and Gases; Hemisphere Publishing Corporation: New York, **1975**.
52. Tong, J. S.; Ma, M. A. *J. Eng. Thermophys.* **1985**, *6*, 11 (In Chinese).